Proceedings of ASME Turbo Expo 2011
GT2011
June 6-10, 2011, Vancouver, British Columbia, Canada

GT2011-45692

FLUID-STRUCTURE INTERACTION USING A MODAL APPROACH

F. Debrabandere
Numflo
Mons, Belgium

B. Tartinville
Numeca International
Brussels, Belgium

Ch. Hirsch
Numeca International
Brussels, Belgium

G. Coussement
University of Mons
Fluid-Machines Department
Mons, Belgium

ABSTRACT

A new method for Fluid-Structure Interaction (FSI) predictions is here introduced, based on a Reduced-Order Model (ROM) for the structure, described by its mode shapes and natural frequencies. A linear structure is assumed as well as Rayleigh damping. A two-way coupling between the fluid and the structure is ensured by a loosely-coupling staggered approach: the aerodynamic loads computed by the flow solver are used to determine the deformations from the modal equations, which are sent back to the flow solver.

The method is firstly applied to a clamped beam oscillating under the effect of von Karman vortices. The results are compared to a full-order model. Then a flutter application is considered on the AGARD wing 445.6. Finally, the modal approach is applied to the aeroelastic behavior of an axial compressor stage. The influence of passing rotor blade wakes on the downstream stator blades is investigated.

INTRODUCTION

An important objective in turbomachinery design is to lighten the structure by the use of specific alloys or composite materials. Because of the complex interactions with the surrounding fluid flow, the capability to analyze Fluid-Structure Interactions (FSI) may be one of the key features in order to achieve such a goal. Hence, blade designers need to have access to efficient and accurate tools so as to predict FSI and aero-elastic instabilities, such as flutter.

Various methods exist to predict fluid structure interactions. Marshall and Imregun [1] divide them into two categories: classical methods and integrated methods. The first ones do not consider the interaction between the fluid and the structure but only the action of one on the other. Hence, it separates the non linear interactions into two set of linear uncoupled phenomena. Such methods are not efficient for turbomachinery design where the interaction between the fluid and the structure are strong and nonlinear. The second ones treat the aeroelastic problem as a whole. It allows the consideration of nonlinear interactions that occur between the fluid flow and the structure deformation. The present approach belongs to this second category.

In the introduced method, the structure is represented by its mode shapes and natural frequencies. The modal equations are solved inside the fluid flow solver in order to retrieve the deformation of the structure and to take it into account in the flow calculation. Compared to other methods using externally coupled solvers [2], it presents the advantage to involve only one solver reducing thereby the complexity of the computational set up.

NOMENCLATURE

$\vec{f}$	= fluid load vector
f	= modal projection of load vector
FSI	= flutter speed index
$\mathbf{I}$	= identity matrix
L_{ref}	= reference length
$\mathbf{M}$	= mass matrix
m_s	= mass of the structure
q	= generalized displacement
$\vec{u}$	= deformation vector
V_f	= free stream velocity at flutter conditions
Vol_{ref}	= reference volume
β, γ	= coefficients of Newmark's algorithm
ξ	= damping ratio
ρ_f	= fluid density
$\vec{\phi}$	= mode shape vector
$\mathbf{\Phi}$	= mode shape matrix
ω	= natural frequency
ω_α	= frequency of 1st torsion mode

Subscripts

k = mode number

n = iteration number

METHOD

The commercial package Fine^{TM}/Turbo [3] is used for this study. This package consists of tools, covering all related parts of Computational Fluid Dynamics (CFD) simulations: a grid generator, a flow solver and a visualization system. All components are adapted to turbomachinery applications. The flow solver is a three-dimensional, density-based, structured, multi-block Navier-Stokes code using a finite volume method. A Radial Basis Function (RBF) interpolation algorithm is used to deform the CFD mesh according to the deformation of the structure [4]. Hence, the Navier-Stokes equations are solved with their Arbitrary Lagrangian-Eulerian (ALE) formulation. Central-difference space discretization is employed for the spatial discretization with Jameson type artificial dissipation. A four-stage explicit Runge-Kutta scheme is applied for the temporal discretization. Multi-grid method, local time-stepping and implicit residual smoothing are used in order to speed-up the convergence.

A structural solver by modal synthesis is integrated inside the flow solver. Using the natural frequencies and the mode shape of the structure, it computes the solid body deformation under the action of fluid loads. The natural frequencies and the mode shapes are determined outside the flow solver and prior to any CFD computation, either by computation with a FEM structure solver or by experiments. In order to avoid any interpolation issues between structure and fluid data [5], the mode shapes defined on a Finite Element mesh are interpolated onto the fluid mesh as suggested by Sayma et al. [6]. A RBF interpolation method is used.

Assuming a linear behavior, a Rayleigh damping, a stiffness not influenced by the frequency and using the normalization $\mathbf{\Phi}^{T}\mathbf{M\Phi} = \mathbf{I}$ for the mode shapes, the structure is characterized by a set of uncoupled modal equations:

$$\frac{\partial^2 q_k}{\partial t^2} + 2\xi_k\omega_k\frac{\partial q_k}{\partial t} + \omega_k^2 q_k = \vec{\phi}_k^T \vec{f} \qquad (1)$$

The fluid load $\vec{f}$ includes pressure and viscous forces acting on the structure.

A common method used to solve these equations is based on the Newmark algorithm [6], [7]. Expressed in variation terms, the iterative resolution of the modal equations is written as:

$$\begin{aligned}
\Delta q_n &= \frac{\Delta f_n + \left(\frac{2\xi\omega\gamma}{\beta} + \frac{1}{\beta\Delta t}\right)\dot{q}_n + \left(\frac{1}{2\beta} + \Delta t\left(\frac{\gamma}{2\beta} - 1\right)\right)\ddot{q}_n}{\omega^2 + \frac{2\xi\omega\gamma}{\beta\Delta t} + \frac{1}{\beta\Delta t^2}} \\
\Delta \dot{q}_n &= \frac{\gamma}{\beta\Delta t}\Delta q_n - \frac{\gamma}{\beta}\dot{q}_n + \Delta t\left(1 - \frac{\gamma}{2\beta}\right)\ddot{q}_n \qquad (2) \\
\Delta \ddot{q}_n &= \frac{1}{\beta\Delta t^2}\Delta q_n - \frac{1}{\beta\Delta t}\dot{q}_n - \frac{1}{2\beta}\ddot{q}_n
\end{aligned}$$

The β and γ parameters are the coefficient of the method, which is unconditionally stable for $\frac{1}{2} \le \gamma \le 2\beta$.

With the assumptions made, a Complementary Function and Particular Integral (CF&PI) method can also be used for the resolution of the modal equation for each mode [8]. With such method, the iterative resolution is directly obtained from:

$$\begin{bmatrix} q_{n+1} \\ \dot{q}_{n+1} \end{bmatrix} = \begin{bmatrix} a_{11} & a_{12} \\ a_{21} & a_{22} \end{bmatrix}\begin{bmatrix} q_n \\ \dot{q}_n \end{bmatrix} + \begin{bmatrix} b_{11} & b_{12} \\ b_{21} & b_{22} \end{bmatrix}\begin{bmatrix} f_n \\ f_{n+1} \end{bmatrix} \qquad (3)$$

The coefficients a_{ij} and b_{ij} depends on the integration time step, the natural frequency and the damping ratio of the mode.

In order to compare the two methods, both are applied to the resolution of the equation:

$$\frac{\partial^2 q}{\partial t^2} + 2\frac{\partial q}{\partial t} + 3q = 10\cos\left(\pi t + \frac{\pi}{4}\right) \qquad (4)$$

This equation is quite similar to Eq. (1) and allows an analytical solution. Therefore, numerical and analytical results are compared on Fig. 1. A numerical time step of 0.1 s has been selected here. It appears that both numerical results fit very well with the analytical solution.

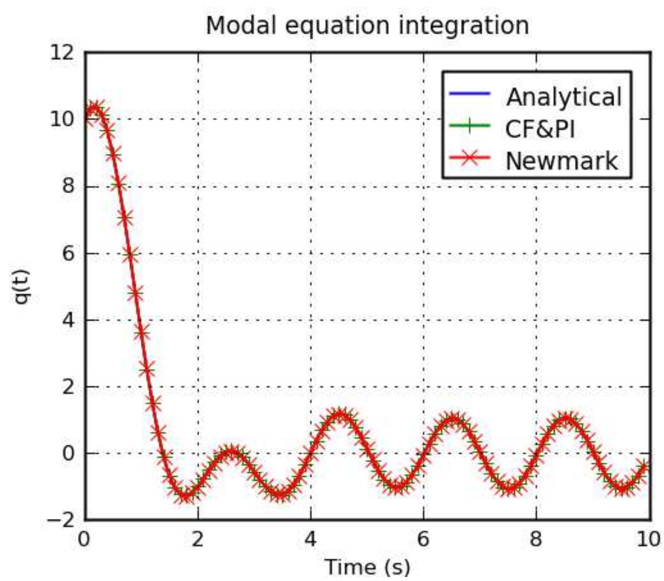

Fig. 1 Comparison of numerical results and analytical solution of Eq. (4)

The differences between the analytical and the numerical solutions are illustrated on Fig. 2. Two different time step sizes are used to verify the second order accuracy of the methods. In both cases the CF&PI method appears to be more precise than the Newmark algorithm. The CF&PI method is then selected for the FSI applications presented in this paper; this constitutes the novel component compared to the work of Sayma et al. [6].

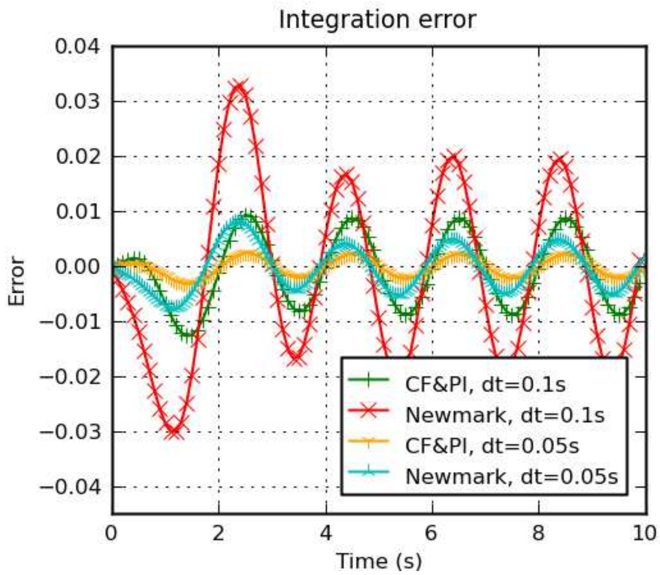

Fig. 2 Numerical error induced by the resolution of Eq. (4) and influence of time step size

After solving Eq. (1) for each structural mode, the structure deformation is retrieved from the calculated generalized displacements by:

$$\vec{u} = \sum_{k=1}^{N_{modes}} q_k \vec{\phi}_k \qquad (5)$$

The two-way coupling between the fluid and the structure is ensured by a staggered approach. The flow computation advances one physical time step. Then the fluid load is sent to the structure solver that computes the corresponding deformation and a new iteration starts. As the equilibrium between the structure and the fluid is not ensured at the end of each iteration, we have a weak coupling method.

APPLICATION

Vortex induced vibration beam

The first application is related to a clamped beam oscillating under the action of von Karman vortices. The computation domain is illustrated in Fig. 3. The flexible beam is characterized by a Young modulus of 2×10^5 Pa, a Poisson's ratio of 0.35 and a density of 2×10^3 kg/m^3. The first five deformation modes are computed with the structural solver Abaqus [9]. Their natural frequencies are equal to 0.7, 4.2, 11.7, 22.9 and 37.7 Hz. The fluid is incompressible air ($\rho = 1.18$ kg/m^3, $\mu = 1.82\times10^{-5}$ Pa s). The laminar flow conditions correspond to a Reynolds number equal to 204. The initial condition is a pseudo-steady solution with a rigid beam.

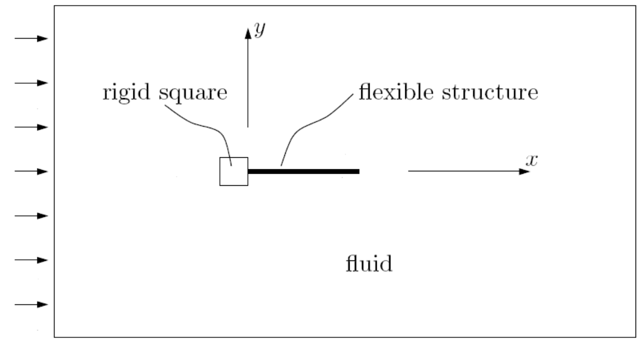

Fig. 3 Vortex induced vibration beam

Due to the rigid square, Von Karman vortices are shed along the beam. It induces pressure variations which lead to the deformation of the flexible structure (Fig. 4). As the beam is very flexible, a small pressure difference is sufficient to produce relatively large deformations.

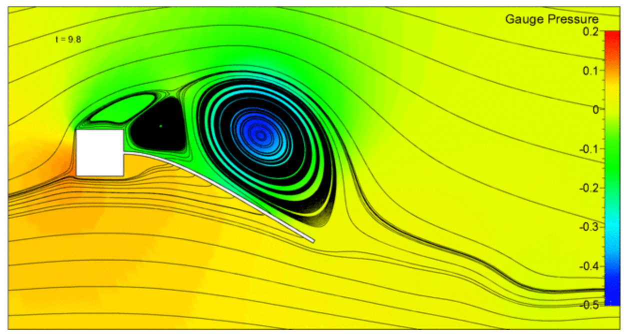

Fig. 4 Instantaneous deformation of the beam at t = 9.8 s

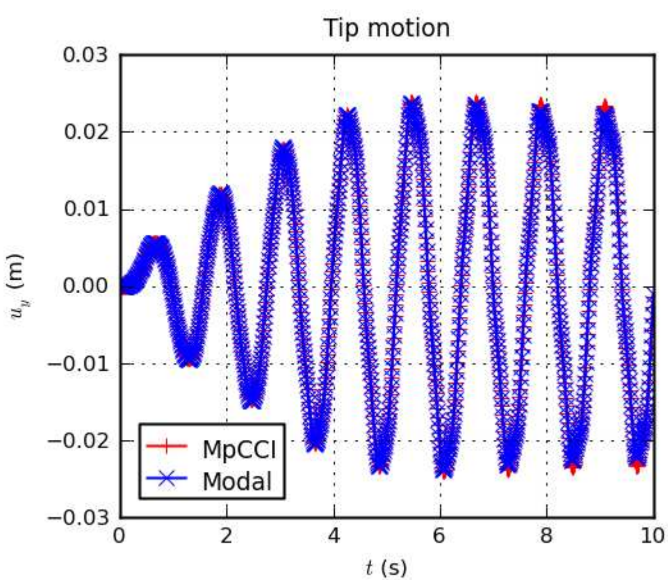

Fig. 5 Tip motion of the beam

The vertical tip displacement of the beam given by the modal approach is depicted on Fig. 5. The first four structural modes are used for the computation. The integration time step is

0.01 s. For comparison, the results obtained with a full order method using the coupling software MpCCI [2] and the structural solver Abaqus are also plotted. Both results are in excellent agreement. The frequency of the periodic oscillations is 0.84 Hz and its amplitude is equal to 0.022 m. These results are in accordance with those obtained by Hübner et al. with a monolithic method [10].

The time evolutions of the generalized displacements are shown on Fig. 6 for the four modes. It can be seen that the first structural mode is predominant. The second mode is also of importance. Its effect can be seen on the tip motion curve which is not purely sinusoidal after the transient step.

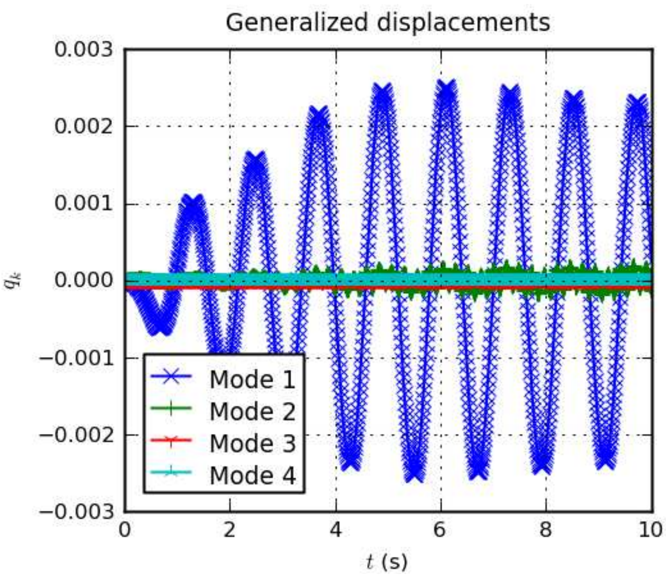

Fig. 6 Generalized displacement of the beam

It has to be noted that the integration time step size must be chosen in accordance with the natural frequency of the highest structural mode. If there are not enough integration points by period, the resolution of Eq. (3) may diverge. It is the case if the same computation is performed with five modes instead of four. The vibration period of this mode is equal to 0.0265 s. Hence an integration time step of 0.01 s is too large for its proper resolution. By reducing the time step, the fifth mode can be accurately solved (not shown).

AGARD wing 445.6

This application is related to the flutter of a wing experimentally studied by Yates [11]. The wing is formed by a NACA65A004 airfoil extruded with a sweep angle of 45° at the quarter chord line and a tapper ratio of 0.6. The structural modal data are directly taken from Yates' publication. The fluid is air considered as perfect gas. The Mach numbers are ranging from 0.5 to 1.14. The root chord based Reynolds numbers vary from 0.46×10^6 to 2.35×10^6. The turbulence is modeled with the Spalart-Allmaras model [12] and extended wall functions [13]. Two fluid domain meshes are used for this application. The first one (named Grid 222) is very coarse with 58,400 nodes. The second one (named Grid 111) is more refined and has 403,200 nodes (Fig. 7).

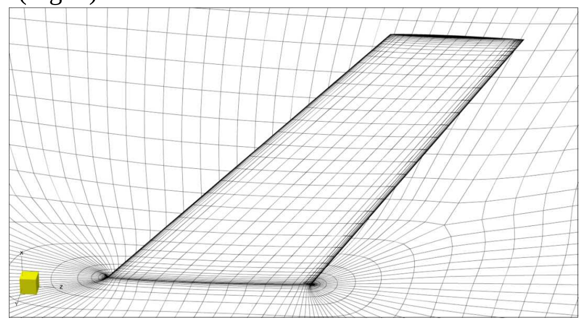

Fig. 7 Mesh used for the AGARD wing 445.6

The flutter conditions are identified by using the same approach as Pahlavanloo [14]. Unsteady FSI computations are performed with different free stream flow conditions. In order to have enough points for the integration of the highest mode, the time step size is set to 5.10^{-4} s. A lift perturbation is imposed during the first 0.05 s. Then the tip motion of the wing is monitored. When it oscillates with constant amplitude the flutter limit is reached (Fig. 8). Otherwise, the free stream static pressure is modified for another computation keeping the Mach number constant.

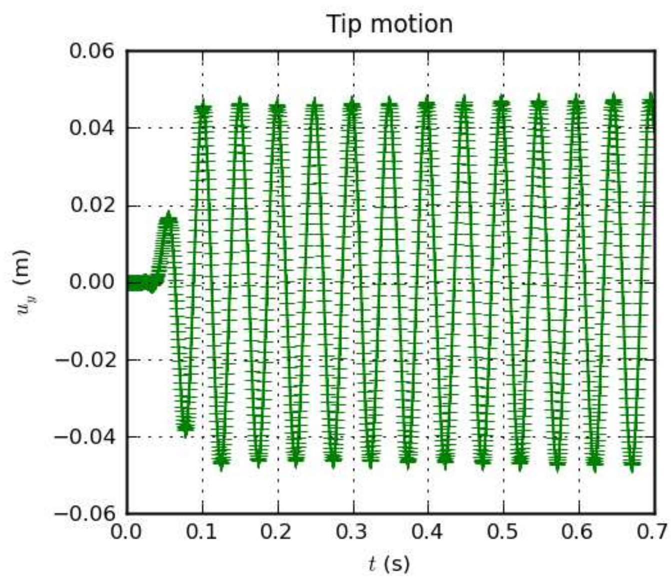

Fig. 8 Tip motion in lift direction at flutter limit at Mach 0.5

The flutter condition is represented by the Flutter Speed Index (*FSI*):

$$FSI = \frac{V_f}{L_{\mathrm{ref}} \omega_\alpha \sqrt{\mu}} \qquad \mu = \frac{m_s}{\rho_f Vol_{\mathrm{ref}}} \tag{6}$$

It includes the ratio between the flow velocity at flutter V_f and the frequency of the first torsion mode ω_α. A ratio between the wing mass and the fluid density at flutter condition appears too.

The computed *FSI* are depicted on Fig. 9. For all Mach numbers considered, the results obtained with the coarsest mesh are higher than those computed with the finest mesh. The gap showing the influence of the mesh is approximately constant and corresponds to about 0.0175 *FSI*. For subsonic flow the results with both meshes are very close to the experimental points. With increasing Mach numbers, the reduction of the *FSI* is well captured by the numerical computations. However the results obtained with the finest mesh underpredict the experimental values. Such underprediction of FSI value at Mach 0.9 and Mach 0.95 is consistent with other studies on the same case [14], [15]. Same behavior is observed for the results on Grid 222 although they appear to be closer to the experimental data due to the constant gap with the results on Grid 111. When reaching supersonic free stream flow, we can see an increase of the experimental *FSI*. However the numerical results at Mach 1.07 have a larger deviation from the data. The current method doesn't succeed to reproduce the experimental behavior for the early supersonic Mach numbers. For the point at Mach 1.14, the increase of FSI is well captured even if the calculated *FSI* are again slightly lower than the experimental value. Such behavior is different from those observed by Pahlavanloo [14] or Beaubien and Nitzche [16] who have numerical values higher than the experimental ones. However, the mode shapes from Yates are not used in the two studies referenced above. Furthermore, the CFD calculations are only performed in Euler and laminar mode, whereas, the present study is based on RANS equations including Spalart and Allmaras turbulence model. The use of such a turbulent closure model should be of importance for transonic application.

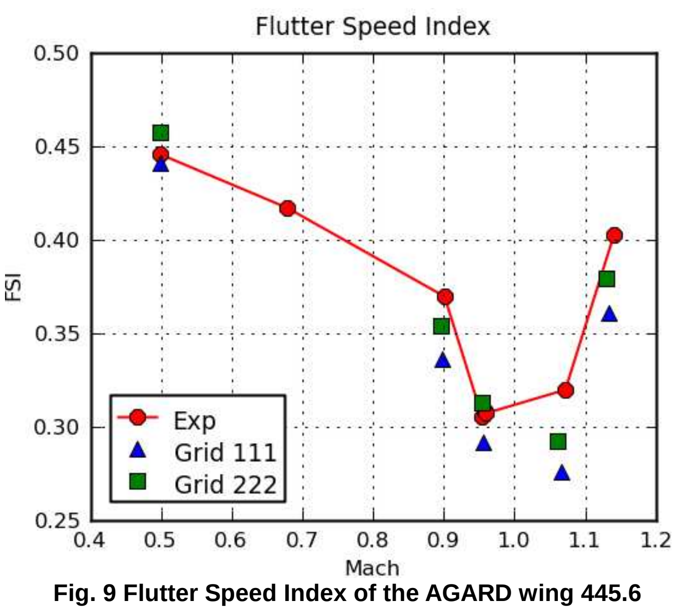

Fig. 9 Flutter Speed Index of the AGARD wing 445.6

The ratios between the frequency of the tip motion and the frequency of the first torsion mode are plotted on Fig. 10. The same observations as for the FSI can be formulated.

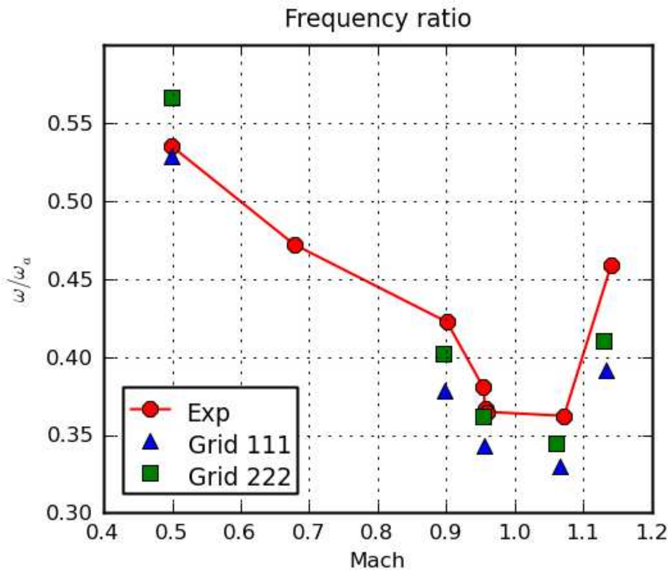

Fig. 10 Frequency ratio of the AGARD wing 445.6

Compressor stage

The last application is related to a rotor-stator compressor stage. The rotor has 16 blades. Its rotation speed equals 20,000 RPM giving a rotor blade passing frequency of 5,333 Hz. In order to reduce the computation domain, the number of stator blades is set to 32. Hence only one blade channel is meshed for the rotor and two for the stator. The computational domain depicted on Fig. 11 is meshed with 146,000 nodes.

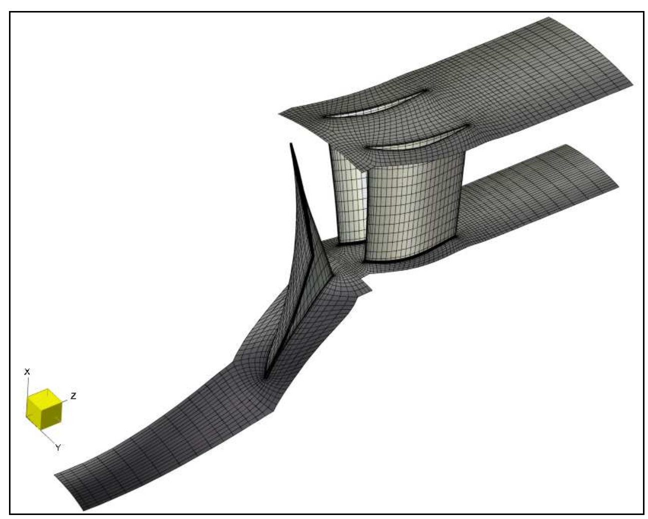

Fig. 11 Geometry and mesh used for the compressor stage

The deformation of the stator blades due to the passing rotor wakes is investigated. Each stator blade is free to deform independently of the other one. The blades are represented by their first ten vibration modes. Their natural frequencies are listed in Tab. 1.

Tab. 1

Mode index	**Frequency** (Hz)
1	1,168
2	2,215
3	4,918
4	5,786
5	7,202
6	8,980
7	9,870
8	10,986
9	12,448
10	17,174

The fluid is air considered as perfect gas. The averaged inlet Mach number is equal to 0.45. The inlet Reynolds number equals 660,000. The Spalart and Allmaras model is used for the turbulence. The unsteady computation is performed with a numerical time step of 4.6875×10^{-6} s in order to have 40 time steps per rotor blade passing period.

The mid-span absolute Mach number field is shown on Fig. 12. As the compressor is transonic, a weak shock is observable at the rotor inlet and a stronger shock between the stator blades.

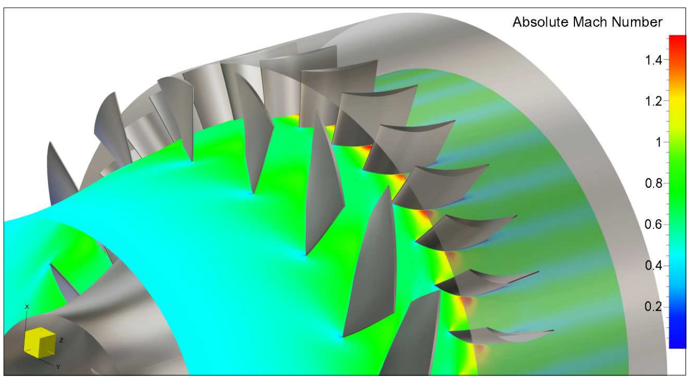

Fig. 12 Absolute Mach number at midspan

The tip displacements at trailing edges of the stator blades are depicted on Fig. 13. The plot window corresponds to five rotor blade passing periods. The deformation fields are also illustrated on Fig. 14 and Fig. 15. A repetition of the computation domain is performed in order to enhance the visualization.

As can be seen, the motion is not identical for both stator blades. The main reason can be found in the phase lag with which the rotor wakes impact the stator blades. However this phase lag doesn't appear between the two motion curves. The time scale of the blade oscillation is different from the blade passing.

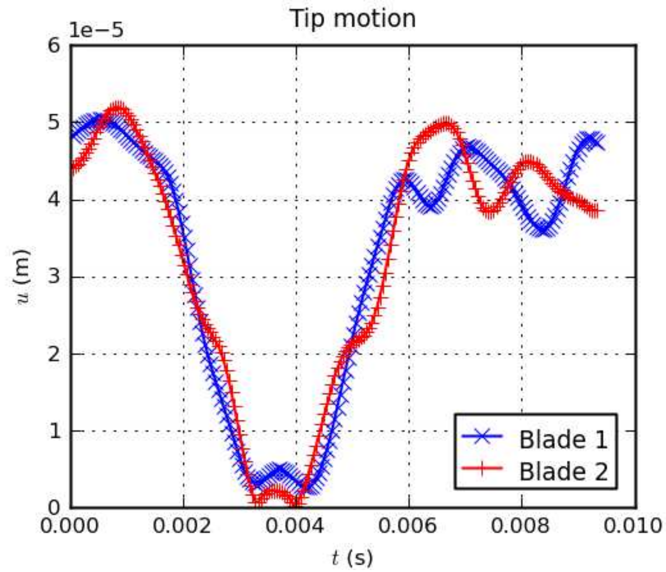

Fig. 13 Tip deformation at trailing edges of the stator

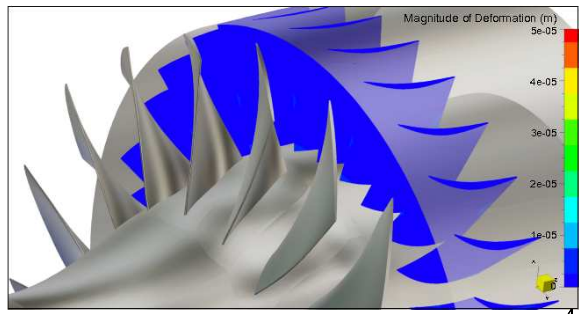

Fig. 14 Deformation of stator blades at t = 3.75×10^{-4} s

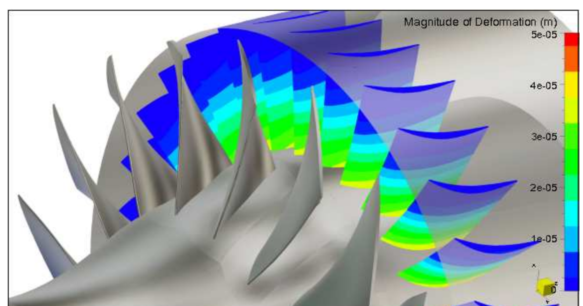

Fig. 15 Deformation of stator blades at t = 8.9×10^{-4} s

The Fourier transform of the tip motion of the first stator blade is depicted on Fig. 16. Several peaks can be observed corresponding to different relevant frequencies. The main peak is observed at 1,185 Hz, near to the natural frequency of the first vibration mode. The second peak is located at 2,253 Hz and corresponds to the frequency of the second vibration mode. Three peaks of smaller amplitude appear around 5,500 Hz. Two of them illustrate the influence of the third and the fourth vibration mode, while the center one is related to the rotor blade passing frequency. To conclude, the passing rotor wakes induce vibrations of the stator blades but the frequency of the vibration is more related to the natural frequency of the blade than to the rotor blade passing frequency.

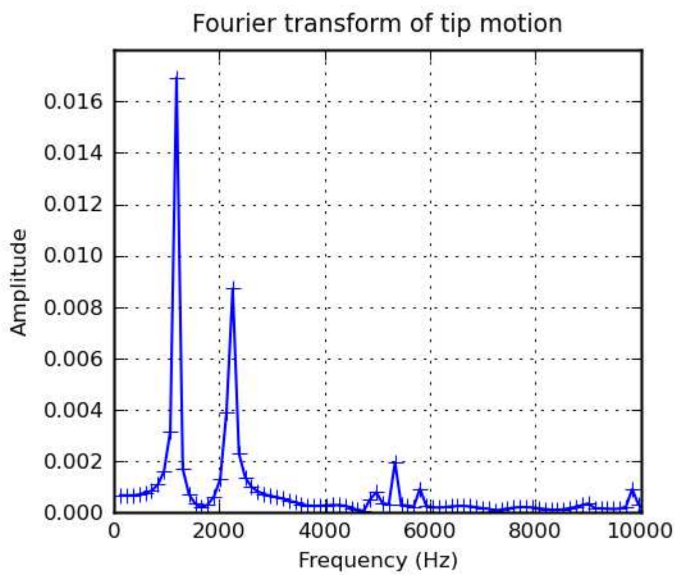

Fig. 16 Fourier transform of the tip motion of the first stator blade

CONCLUSIONS

A method for FSI prediction has been developed. It uses a reduce order model based on a modal synthesis for the structure. The computation of the structure deformations is directly performed by the flow solver in order to avoid data interpolation issues between structural and fluid meshes. The modal equations are solved by a complementary function and particular integral method which appears to be more accurate than Newmark's algorithm.

The method has been applied with success to several configurations. The computed vibration of a simple clamped beam under the action of von Karman vortices are the same as those computed by other numerical methods. The method allows the computation of flow conditions leading to the flutter of a wing with results in accordance with the experiment. Finally, the last application illustrates the usability of the method for the prediction of blade motions due to passing wakes in turbomachines.

Stability issues have been found when the integration time step size is too large regarding the frequency of the highest mode used for the structural computation. As a rule it seems that the integration time step size must be smaller than one third of this frequency.

Despite this limitation, the method introduced in this paper appears to be a simple and efficient approach for the FSI prediction even for complex configuration such as compressor stage. It will be used in a future work for the analysis of the flutter and the forced response in turbomachinery. It will be the opportunity to investigate the influence of the computational time step size and the blade passing frequency regarding to the frequencies of the structure vibration modes.

A further extension is the coupling of this FSI approach with the Nonlinear Harmonic method [17] for general rotor-stator interactions.

REFERENCES

[1] Marshall, J. G., Imregun, M., "A Review of Aeroelasticity Methods with Emphasis on Turbomachinery Applications", Journal of Fluids and Structures 10 (1996), 237–267.

[2] SCAI, "MpCCI User Manual v3.0.6", 2007.

[3] NUMECA International, "User Manual Fine^{TM}/Turbo v8", 2007.

[4] de Boer, A., van der Schoot, M. S., Bijl, H., "Mesh deformation based on radial basis function interpolation", Computers and Structures 85 (2007), 784–795.

[5] Fenwick, C. L., Allen, C. B., "Flutter Analysis of the BACT Wing with Consideration of Control Surface Representation", 25th AIAA Applied Aerodynamics Conference (2007), AIAA 2007-3805.

[6] Sayma, A. I., Vahdati, M., Imregun, M., "An Integrated Nonlinear Approach for Turbomachinery Forced Response, Part I: Formulation", Journal of Fluids and Structures 14 (2000), 87–101.

[7] Humar, J. L., "Dynamics of structures", 2nd Ed., Swets & Zeitlinger, 2001, ISBN 90-5809-254-3.

[8] Boyce, W. E., DiPrima R.C., "Elementary Differential Equations and Boundary Value problems", 7th Ed., John Wiley & Sons, 2000, ISBN 04-7131-999-6.

[9] DS Simulia, "Abaqus Analysis User's Manual Version 6.8", 2008.

[10] Hübner, B., Walhorn, E., Dinkier, D., "A Monolithic Approach to Fluid-Structure Interaction Using Space-Time Finite Elements", Comput. Methods Appl Mech. Engrg., 193 (2004), 2087–2104.

[11] Yates, E. C., "AGARD Standard Aeroelastic Configurations for Dynamic Response. Candidate Configuration I.-wing 445.6", 1987, NASA-TM-100492.

[12] Spalart, P. R., Allmaras, R., "A One-Equation Turbulence Model for Aerodynamic Flows", La Recherche Aerospatiale N. 1 (1994), 5–21.

[13] Kalitzin, G., Medic, G., Iacaarion, G., Durbin, P., "Near-Wall Behavior of RANS Turbulence Models and Implications for Wall Functions", Journal of Computational Physics 204 (2005), 265–291.

[14] Pahlavanloo, P., "Dynamic Aeroelastic Simulation of the AGARD 445.6 Wing Using Edge", 2007, FOI-R—2259--SE

[15] Haase, W., Selmin, V., Winzell, B., "Progress in Computational Flow-Structure Interaction: results of the project UNSI supported by the European Union 1998-200", Springer, 2003, ISBN 3-540-43902-1.

[16] Beaubien, R. J., Nitzsche, F. "Time and Frequency Domain Flutter Solutions for the AGARD 445.6 Wing", 2005, Paper IF-102, IFASD.

[17] Vilmin, S., Lorrain, E., Hirsch, Ch., Swoboda, M., Unsteady Flow Modeling Across the Rotor/Stator Interface Using the Nonlinear Harmonic Method, ASME Turbo Expo 2006, GT2006-90210.